MEASUREMENT SCIENCE REVIEW, **26**, (2026), No. 1, 1-9

De Gruyter Brill
Paradigm
ISSN 1335-8871

MEASUREMENT SCIENCE REVIEW

Journal homepage: https://reference-global.com/journal/MSR

Enhancing the Performance of Pulse Position Coded Excitation for Photoacoustic Imaging by Denoising Autoencoder

Abdulrhman Alshaya[1]*#, Suhail Alshahrani[2]#

[1]King Abdulaziz City for Science and Technology (KACST), Riyadh, 12354, Saudi Arabia, aaalshaya@kacst.gov.sa
[2]Department of Biomedical Technology, College of Applied Medical Sciences, King Saud University (KSU), Riyadh,12372, Saudi Arabia, suhailsalem@ksu.edu.sa
#Equal Contribution

Abstract: Photoacoustic (PA) imaging is a hybrid technique that combines light illumination and ultrasound detection to generate images of tissue. Advances in laser technology allow laser diodes that are low cost, compact, and have a high pulse repetition frequency (PRF) to improve the frame rate and signal-to-noise ratio (SNR) of PA imaging. This improvement is achieved by employing PA-coded excitation techniques. However, PA-coded excitation is limited by side-lobes and artifact signals, particularly when the code length is short. Pulse position modulation (PPM) is a type of coded excitation that achieves the highest code gain with a short code length. This study explores a signal-processing approach that integrates PPM-coded excitation with a denoising autoencoder to reduce the generated side lobs and artifact signals and enhance the SNR of the PA signals. The denoising autoencoder is designed to address the varying shapes of side lobes that occur with different PPM code lengths, resulting in improved attenuation and removal of artifacts and background noise. The results show that the denoising autoencoder is particularly effective when the amplitude of the decoded PA signal exceeds that of the background noise, enabling reduced acquisition time and memory requirements for RF data collection. This work offers a promising approach to overcoming the limitations of PPM-coded excitation in PA imaging, supporting further improvements in the quality and reliability of PA signals for various medical applications.

Keywords: photoacoustic imaging, pulse position modulation, denoising autoencoder, averaging technique, signal-to-noise ratio, artifact reduction

1. INTRODUCTION

Photoacoustic (PA) imaging, also known as optoacoustic imaging, is a hybrid technique that generates images by combining optical light and ultrasound detection [1]. This method involves illuminating biological tissue with a short-pulse laser. The light is absorbed by optically active molecules within the tissue. This absorbed light energy is converted into heat, causing rapid thermal expansion and generating acoustic waves known as PA waves, which are detected by ultrasound transducers [2]. PA imaging has a range of applications in the medical field, including biomedical research and clinical diagnostics. For example, it can monitor tumor angiogenesis, map blood oxygenation, and perform functional brain imaging. Additionally, it is used to detect skin melanoma and measure methemoglobin levels [2], [3].

Significant advances in laser technology have revolutionized the capabilities of PA imaging. Various pulsed lasers, such as Nd: YAG lasers, dye lasers, and semi-conductor lasers, have contributed to the development of the PA imaging field. Nd: YAG lasers are known for their high energy, short pulse duration, and excellent beam quality. However, they also have limitations, including high cost, large size, and a low pulse repetition rate (approximately 10 Hz), which can affect the imaging frame rate [4], [5]. In contrast, semiconductor lasers, such as diode lasers, are compact, cost-effective, and can be directly modulated. Despite these advantages, diode lasers often have low output energy and limited beam quality [4], [6], [7]. To overcome diode laser limitations, various signal-processing techniques, including averaging techniques and coded excitation methods, may be used in image processing, particularly for image denoising, enhancement, and ultrasound/PA imaging [8]. Although averaging is limited by the acoustic signal's flight time, PA-coded excitation (PACE) provides a viable solution to this limitation [9], [10].

Pulse position modulation (PPM) is a type of coded excitation method that has been applied to PA imaging. This type of coded excitation achieves the highest code gain with a short code length [11]. However, artifact signals associated

DOI: 10.2478/mr-2026-0001

*Corresponding author: aaalshaya@kacst.gov.sa (A. Alshaya) with the PPM coding method are a well-documented challenge that can negatively affect the quality and reliability of PA signals [12]. To address this limitation, this study will explore a signal processing approach that integrates the PPM-coded excitation technique with a denoising autoencoder to reduce artifact signals in the decoded PA signals and improve the signal-to-noise ratio (SNR).

2. MATERIALS & METHODS

A. *Pulse position modulation*

As mentioned earlier, PPM is a type of coded excitation method that has been applied to PA imaging [11]. PPM relies on the time shift between the sequence of transmitted laser pulses, as shown in Fig. 1. In this method, the pulse repetition interval between the first two laser pulses is designated as τ_L. Subsequently, the pulse repetition interval increases by a small time step (τ_s) as the code length increases [11].

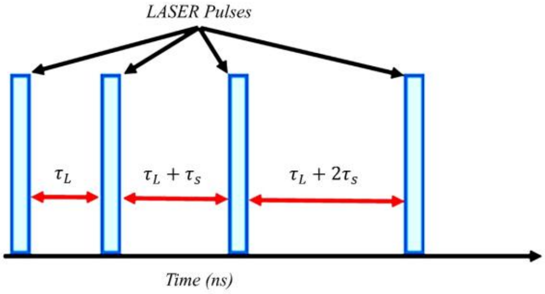

Fig. 1. Schematic of the transmitted laser pulse sequence for PPM.

The increment in the pulse repetition interval should not exceed the flight time of the acoustic signal from the maximum target depth (τ_E) to achieve maximum code gain ($N_{\max}$). The maximum code length to obtain maximum code gain ($N_{\max}$) can be calculated using (1) [11].

$$N_{\max} = \sqrt{2\frac{\tau_E - \tau_L + 2\tau_s}{\tau_s}} \qquad (1)$$

When laser pulse sequences of PPM are transmitted to the imaging target, sequences of PA signals are received by the ultrasound transducer. However, these signals contain both the actual PA signals and noise. To extract the actual PA signal, the received PA signal sequence is convolved with the inverse transmitted PPM code sequence, as shown in (2) [11].

$$y_{\mathrm{PPM}}(k) = (A_{\mathrm{ph}}(k) * h_{\mathrm{sys}}(k) + n(k)) * A(-k) \qquad (2)$$

Here, $y_{\mathrm{PPM}}(k)$ is the decoded PA signal, $A_{\mathrm{ph}}(k)$ is the generated sequence of PA signals, $h_{\mathrm{sys}}(k)$ is the impulse response of the system, $n(k)$ is the background noise, and $A(-k)$ is the inverse transmitted PPM code sequence.

B. *Denoising autoencoder*

In general, the autoencoder is a type of neural network based on unsupervised learning algorithms [13]. An autoencoder neural network consists of two parts: the encoder and the decoder. In the encoder part, the dimension of the input signal is reduced, and its features are learned. In the decoder part, the input signal is reconstructed from the dimensional reduction signal based on the learned features. Through this process, the autoencoder neural network learns to reconstruct the input signal with minimal loss, making it as similar as possible to the original input signal [13], [14]. The denoising autoencoder, a special type of autoencoder, is used to improve the SNR of the input signal by compressing the background noise signal (unwanted signal). In the denoising autoencoder, the input signal is a noisy signal consisting of the original signal combined with a random noise signal. This noisy signal is compressed, and its features are learned in the encoder part. The denoised signal is then reconstructed from the compressed signal based on the learned features in the decoder part. This reconstruction process is trained to minimize the loss value between the original and reconstructed signals (denoised signal), as shown in Fig. 2 [13]-[15].

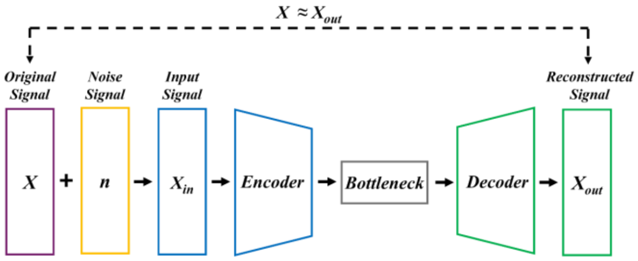

Fig. 2. The diagram shows the process of the denoising autoencoder.

C. *Combination of PPM and denoising autoencoder*

The main objective of the proposed method is to reduce artifact signals in the decoded PA signals generated by PPM-coded excitation, thereby enhancing the SNR of these signals. This will be accomplished by integrating the PPM-coded excitation technique with a denoising autoencoder neural network, as shown in Fig. 3. In this approach, the decoded PA signal from the PPM-coded excitation is input into the denoising autoencoder neural network (denoted as $y(k)_{in}$), which compresses the input signal and extracts its features. The compressed signal is then reconstructed (denoted as $y(k)_{out}$) based on the learned features. The reconstructed signal is evaluated against the original signal $X(k)$ using the mean square error metric. This iterative process continues until the denoising autoencoder model achieves an acceptable mean square error value.

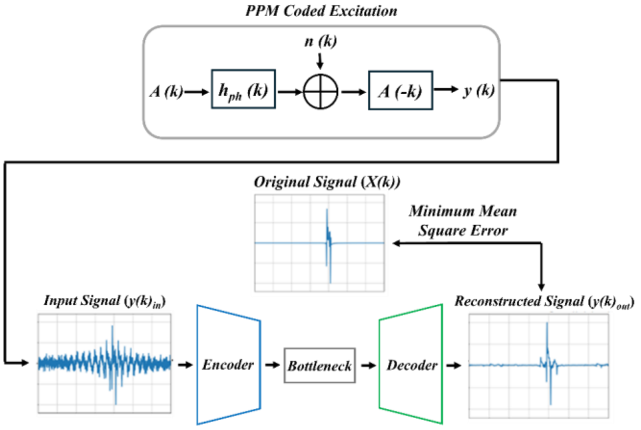

Fig. 3. The combination of the coded excitation technique and the denoising autoencoder neural network.

D. *Numerical simulation and experiments*

Simulation setup

A K-wave toolbox [16], [17] was used to generate PA emissions for training a denoising autoencoder model. The PA emissions were produced by multiple absorbers with varying sizes (radii ranging from 0.1 mm to 2 mm), different positions relative to the transducer (distances from 10 mm to 60 mm), and distinct initial pressure distributions (ranging from 0.3 Pa to 2 Pa), as shown in Fig. 4. A 128-element linear transducer with a central frequency of 5 MHz and a bandwidth of 90 % at –6 dB was used to receive the generated PA emissions. The grid size in this simulation was 0.1 mm. The speed of sound in the simulation medium was set to 1500 m/s, and the sampling frequency was 40 MHz. In the PPM-coded excitation, the laser pulse repetition frequency (PRF) and increment step were 500 kHz and 25 seconds, respectively.

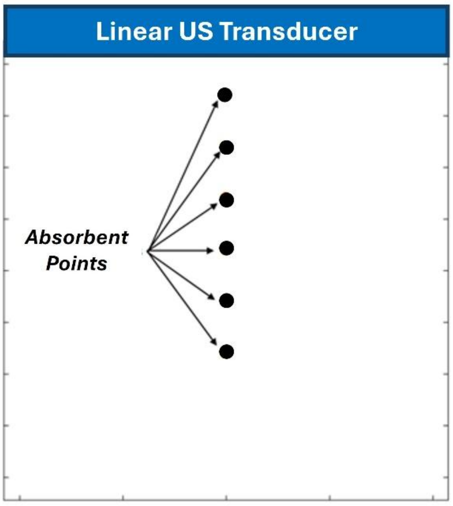

Fig. 4. The graph shows a sample of the simulation setup.

The PPM-coded excitation with different code lengths was applied to 4,608 RF signals generated using the K-wave toolbox. This coded excitation produces coded artifacts (side lobes) in the decoded PA signal. The shape and amplitude of these coded artifacts are influenced by the code length of the PPM-coded excitation, as shown in Fig. 5. Specifically, Fig. 5(a) presents the original PA signal generated from six absorbers, while Fig 5(b) and Fig. 5(c) show the decoded PA signal without background noise. In the coded PA signals shown in Fig. 5(b) through (d), the amplitude of the coded artifacts (side lobes) decreases as the code length increases. Furthermore, both the distribution and shape of these artifacts are affected by the code length and the shape of the imaging targets.

It is important to note that background noise was added to the generated sequence of PA signals to achieve a SNR of –10 dB (rms) before decoding. Fig. 6 shows the original PA signal and the decoded PA signal from PPM-coded excitation after the addition of background noise.

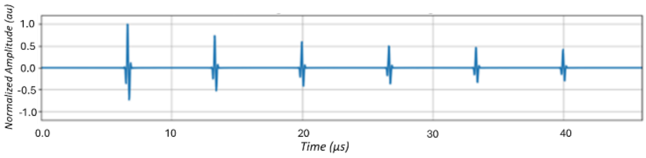

(a) The generated PA signal.

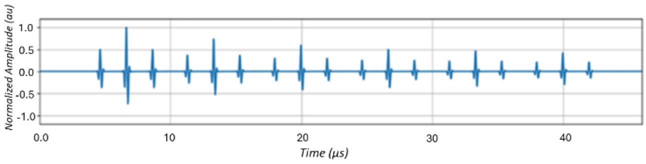

(b) The PA signal that results of PPM coded excitation (N=2).

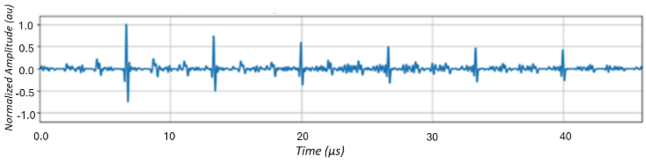

(c) The PA signal that results of PPM coded excitation (N=14).

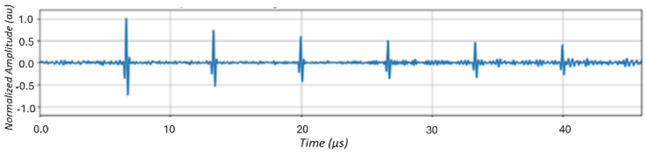

(d) The PA signal that results of PPM coded excitation (N=56).

Fig. 5. (a) The original PA signal, (b) The coded PA signal from PPM with a code length of 2, (c) 14, and (d) 56.

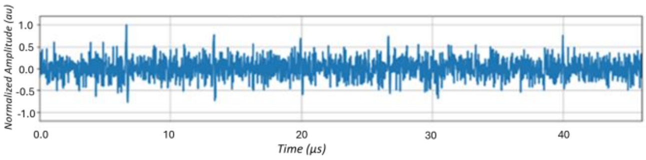

(a) The generated PA signal.

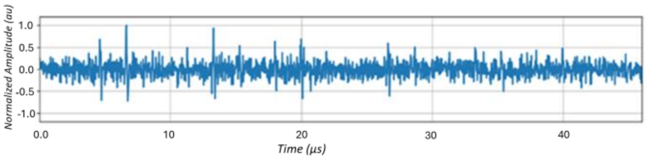

(b) The PA signal that results of PPM coded excitation (N=2).

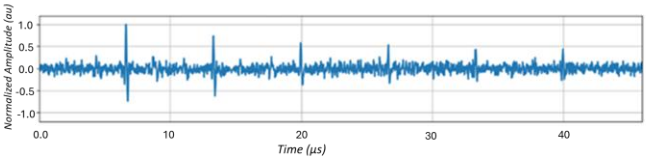

(c) The PA signal that results of PPM coded excitation (N=14).

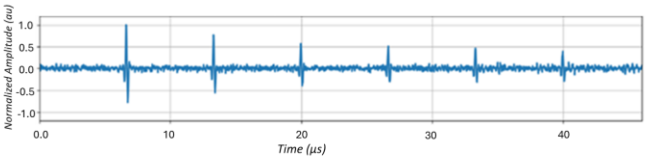

(d) The PA signal that results of PPM coded excitation (N=56).

Fig. 6. (a) Original PA signal with a –10 dB (rms) SNR, (b) Decoded PA signal from PPM-coded signals with code lengths of 2, (c) 14, and (d) 56, after introducing noise to the generated PA sequence (–10 dB SNR (rms)).

The denoising autoencoder was designed and implemented using TensorFlow, an open-source framework for deep learning. This neural network architecture was specifically structured to process one-dimensional RF data as performed in literature [13]. The input layer contains 1864 nodes, corresponding to the number of input signal samples. The encoder component consists of three convolutional layers, three max-pooling layers, and two dropout layers, as shown in Fig. 7. The decoder includes three up-sampling layers followed by three convolutional layers. All convolutional layers use the rectified linear unit (ReLU) activation function [18]. The max-pooling layers down-sample the data by a factor of two, retaining the maximum value within a window of two samples. The dropout layers, which help prevent overfitting, randomly deactivate 20 % of the nodes during training [19]. The up-sampling layers are designed to reconstruct the input data by doubling the sample rate. The loss between the original and reconstructed signals is measured using the mean squared error (MSE) metric. Based on the computed loss, the weights of the nodes are adjusted, and the neural network model is iteratively retrained.

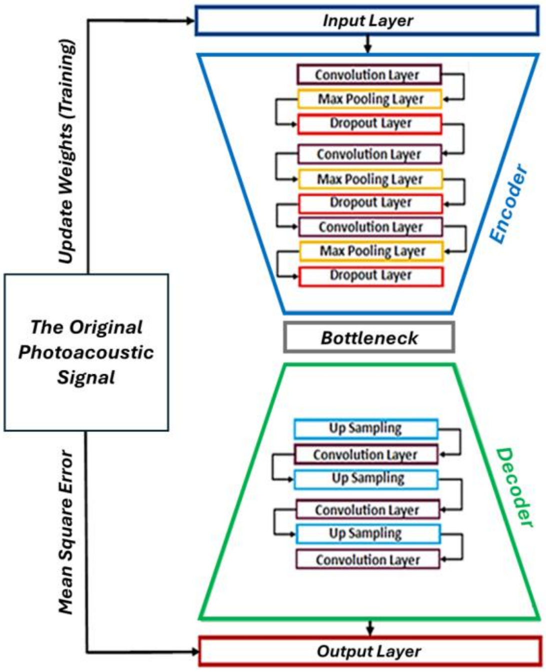

Fig. 7. The graph illustrates the structure of the denoising autoencoder training process.

In this study, a separate training model was developed for each PPM code length. For each training model, the input signal for the denoising autoencoder was the decoded PA signal from the PPM-coded excitation. The loss function, calculated as the MSE, was the difference between the reconstructed signal (output signal) and the original PA signal (without background noise). The Adam optimization algorithm was used, and the model was trained for 80 epochs. The dataset was divided, with 80 % used for training and 20 % reserved for testing. Table 1 summarizes the denoising autoencoder model parameters. The initial training loss was 0.0175, which decreased to 0.00003 by the 80th training epoch. This demonstrates that the model effectively denoised the PA signals and reconstructed the original signals with high fidelity.

Table 1. Denoising autoencoder model summary.

Layer (type)	Output shape	Param # [1]
Encoder (sequential)	(None, 1, 233, 8)	6456
Decoder (sequential)	(None, 1, 1864, 1)	12209

[1] Total params: 18665 (72.91 KB),
[2] Trainable params: 18665 (72.91 KB),
[3] Non-trainable params: 0 (0.00 Byte).

Simulation experiments

Two simulation setups were used to test the performance of PPM-coded excitation with a denoising autoencoder model. The first simulation setup consists of a single absorber, as shown in Fig. 8(a), and is used to compare PPM and PPM with a denoising autoencoder in terms of SNR and code gain for the decoded PA signals.

In this setup, SNR and code gain were calculated for the PA signal received by transducer element number 64 (Mid of linear transducer). SNR was calculated using (3) [20].

$$SNR_{\mathrm{dB}} = 20\log_{10}\frac{S_{\mathrm{RMS}}}{N_{\mathrm{RMS}}} \tag{3}$$

where S_{RMS} is the root mean square of the target signal and N_{RMS} is the root mean square of the noise signal. The region of interest (ROI) for the signal and noise used to calculate SNR is shown in Fig. 8(b).

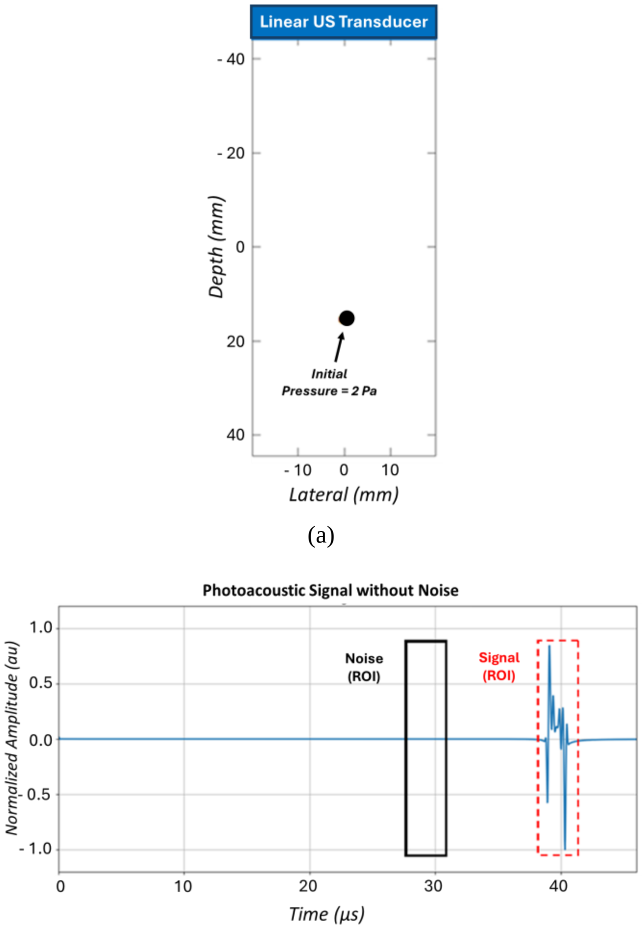

(a)

(b)

Fig. 8. (a) The first simulation setup for testing PPM with denoising autoencoder models; (b) the ROI of the PA signal used to calculate SNR.

The second simulation setup was used to evaluate the performance of PPM and PPM with a denoising autoencoder for multiple absorbers (six absorbers), as shown in Fig. 9(a). The regions of interest (ROIs) for signal and noise used to calculate SNR are shown in Fig. 9(b), while the specifications of the absorbent points are shown in Table 2. In both simulation setups, the generated PA signals were received by a 128-element linear transducer array with a center frequency of 5 MHz and a bandwidth of 4.5 MHz (90 % of the center frequency). Before applying the denoising autoencoder model to the decoded PA signals, noise signals were added to the received coded PA signals to achieve an SNR of –10 dB (rms).

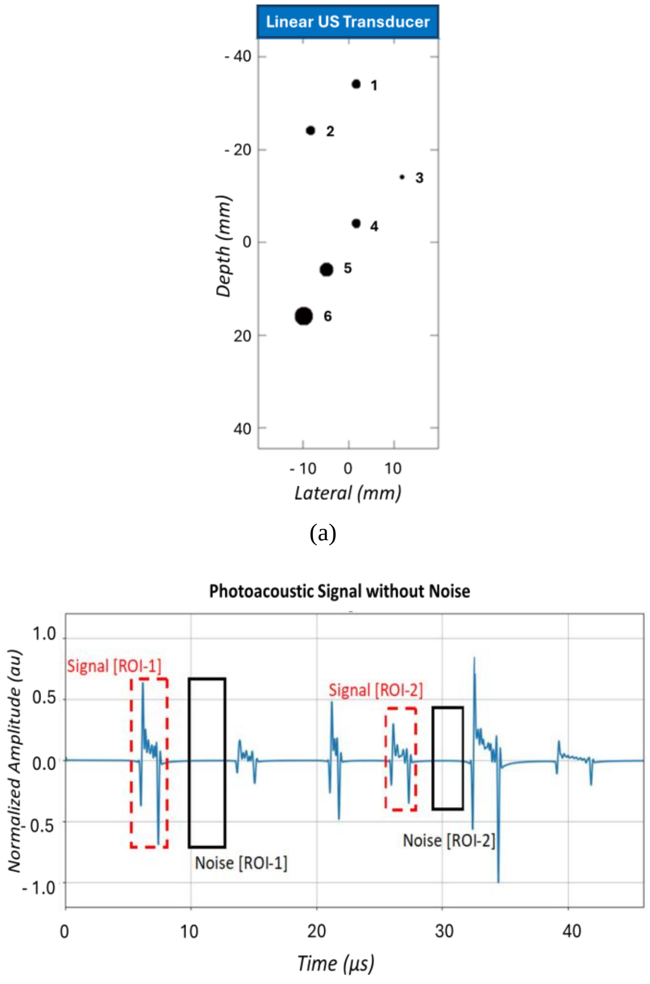

(a)

(b)

Fig. 9. (a) The second simulation setup for testing PPM with denoising autoencoder models. (b) The ROIs of the PA signal are used to calculate SNR. The red dashed boxes and black boxes in this figure indicate the signal and noise regions, respectively.

Table 2. The specifications for absorbent points.

Absorbent point	Radius [mm]	Initial pressure [Pa]
1	1	2
2	1	1
3	0.5	4
4	1	2
5	1.5	5
6	2	1

3. RESULTS

A. *Testing PPM with denoising autoencoder model (single absorber)*

The comparison between PPM-coded excitation and PPM-coded excitation with a denoising autoencoder, in terms of code length and SNR, is illustrated in Fig. 10. In this simulation, ten samples of PA signals were analyzed to determine the mean and standard deviation of SNR for each code length. The maximum code length considered was 56, which is the maximum code length required to achieve maximum code gain based on the averaging technique. The results show that PPM-coded excitation combined with a denoising autoencoder significantly enhances SNR compared to PPM-coded excitation alone. Furthermore, using PPM with a denoising autoencoder achieves higher SNR at shorter code lengths. For example, with a code length of 10, the mean SNR was 23.7 dB and the standard deviation was 7.3 dB when employing the denoising autoencoder. In contrast, using PPM alone at the maximum code length of 56 resulted in a mean SNR of only 8.4 dB and a standard deviation of 0.83 dB.

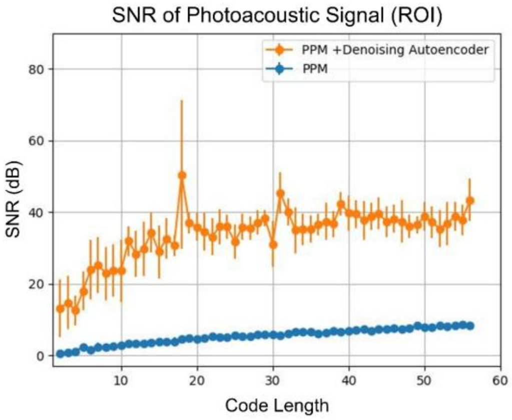

Fig. 10. The relationship between code length and SNR of PPM and PPM with denoising autoencoder for the signal absorber.

Fig. 11 shows a comparison between PPM-coded excitation and PPM-coded excitation with a denoising autoencoder, focusing on code gain as determined by the averaging technique. The results show that the denoising autoencoder enhances the code gain of PPM-coded excitation. Specifically, using PPM with a denoising autoencoder achieves higher code gain with a shorter code length. For example, when PPM-coded excitation is used with a code length of 10, the mean code gain is 23 dB with a standard deviation of 6.8 dB. In contrast, using PPM with a code length of 56 results in a mean code gain of only 6.5 dB and a standard deviation of 1.1 dB. The simulation results show that the standard deviation of both the SNR ratio and code gain is significantly higher when employing PPM-coded excitation with a denoising autoencoder compared to using PPM-coded excitation alone. This increased variability is attributed to the highly correlated background noise generated during the decoding process of PPM-coded excitation. Such correlated noise can amplify artifact signals (side lobes) depending on their position. The denoising autoencoder helps to slightly reduce this correlated background noise, contributing to the observed fluctuations in SNR and code gain.

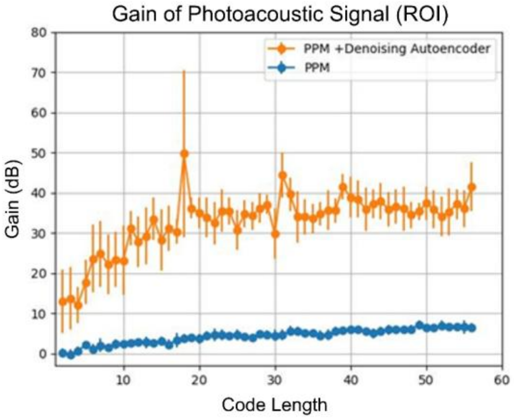

Fig. 11. The relationship between code length code gain for PPM-coded excitation and PPM-coded excitation withdenoising autoencoder for the signal absorber.

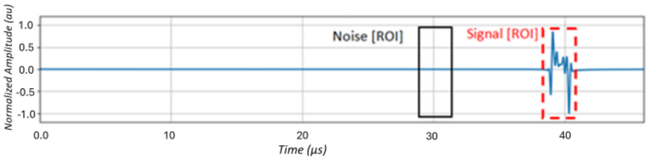

(a) PA signal without noise.

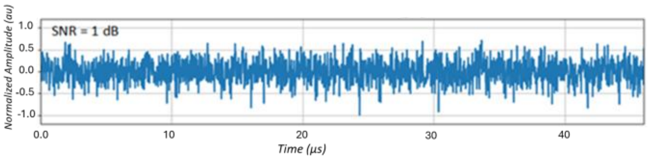

(b) Time-equivalent averaging.

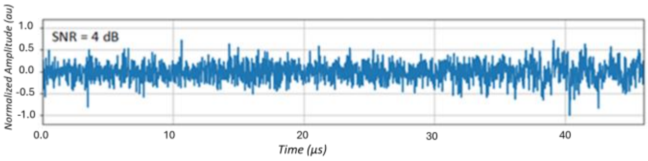

(c) PPM (N=10).

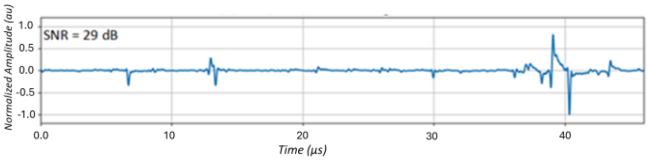

(d) PPM (N=10) and denoising autoencoder.

Fig. 12. (a) The original PA signals, a PA signal resulting from (b) Time-equivalent averaging, (c) PPM (N = 10) coded excitation, and (d) PPM (N = 10) coded excitation with denoising autoencoder.

Fig. 12 presents a comparison of PA signals obtained from three different techniques: PPM, PPM with a denoising autoencoder, and time-equivalent averaging, all using a code length of 10. The results show that PPM with the denoising autoencoder improved the SNR by 25 dB compared to standard PPM and by 28 dB compared to the time-equivalent averaging technique. Additionally, the denoising autoencoder effectively reduced noise and artifact signals (side lobes) generated by PPM, as shown in Fig. 12(c) and Fig. 12(d). However, some parts of the artifact signal remained after using the denoising autoencoder (Fig. 12(d)). This is due to the combination of highly correlated background noise with artifact signals generated during the PPM decoding. As a result, the denoising autoencoder could not differentiate between the actual PA signal and the artifact signal.

However, the impact of highly correlated background noise decreases as the PPM code length increases, as shown in Fig. 13(a). For instance, when the PPM code length is increased to 56, the SNR for PPM improves by 7.64 dB compared to the time-equivalent averaging technique (Fig. 13 (b)). Despite this improvement, side-lobe signals remain in the decoded PA signal for PPM with a code length of 56 (Fig. 13(c)). Applying a denoising autoencoder significantly reduces these side-lobe signals, as shown in Fig. 13(d), resulting in an additional SNR enhancement of 30 dB.

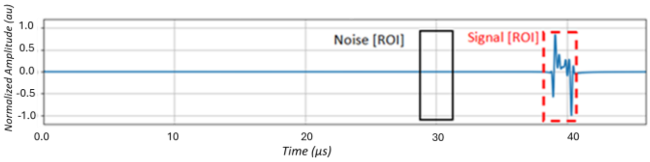

(a) PA signal without noise.

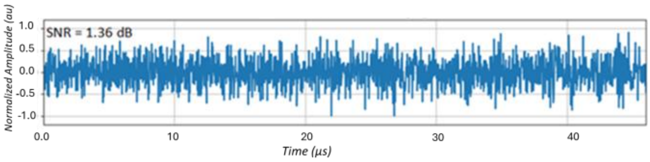

(b) Time-equivalent averaging.

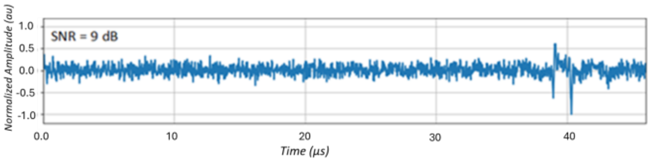

(c) PPM (N=56).

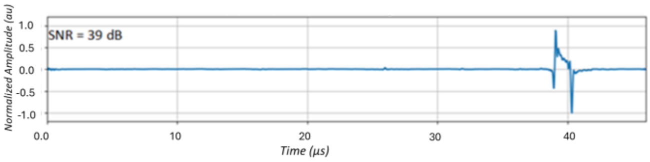

(d) PPM (N=56) and denoising autoencoder.

Fig. 13. (a) The original PA signals, a PA signal resulting from (b) Time-equivalent averaging, (c) PPM (N = 56) coded excitation, and (d) PPM (N = 56) coded excitation with denoising autoencoder.

B. *Testing PPM with denoising autoencoder model (multiple absorbers)*

The impact of code length on the SNR of decoded PA signals generated by PPM and PPM with a denoising autoencoder for regions of interest (ROI-1 and ROI-2) is illustrated in Fig. 14(a) and Fig. 14(b), respectively. SNRs were calculated using (3), with ten samples used to compute the mean and standard deviation for each code length. In Fig. 14(a), the SNR of the decoded PA signal from PPM-coded excitation shows significant improvement across all code lengths for ROI-1 when a denoising autoencoder is applied. For example, at a code length of 10, the denoising autoencoder improves the SNR by approximately 9.8 dB (mean). When the code length increases to 56, the improvement in SNR reaches nearly 28 dB (mean). In contrast, for ROI-2, the denoising autoencoder does not improve the SNR of the decoded PA signal when the code length is short (less than 13). For instance, at a code length of 7, the SNR decreases by almost 1.7 dB (mean) after applying the denoising autoencoder. This reduction occurs because the low SNR of the decoded signal prevents the denoising autoencoder from effectively distinguishing between actual PA signals and background noise. The effectiveness of the denoising autoencoder is evident when the amplitude of the decoded PA signal is relatively higher than that of the background noise before its application. For example, at a code length of 56, the SNR of the decoded PA signal for ROI-2 is approximately 3 dB (mean), as shown in Fig. 14(b). Consequently, applying the denoising autoencoder results in an SNR improvement of nearly 22 dB.

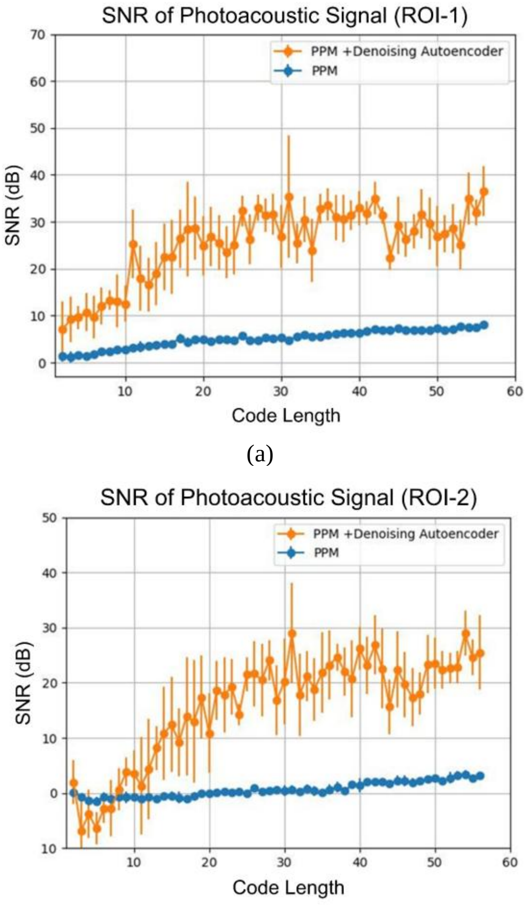

Fig. 14. The relationship between code length and SNR of PPM and PPM with a denoising autoencoder for (a) ROI-1 and (b) ROI-2.

Fig. 15 and Fig. 16 show samples of PA signals generated using PPM, PPM with a denoising autoencoder, and time-equivalent averaging, with code lengths of 10 and 56, respectively. Fig. 15(a) shows the original PA signals along with the ROIs for signal (red dashed boxes) and noise (solid black boxes) used to calculate the SNR. The SNR for the time-equivalent averaging signal (Fig. 15(b)) with a PPM code length of 10 for ROI-1 and ROI-2 is 1.4 dB and –0.7 dB, respectively. This low SNR is due to the short code length, which is equivalent to one-time averaging. When PPM (N = 10) is used, the SNR values for ROI-1 and ROI-2 are 3.5 dB and –1.4 dB, respectively. Notably, the SNR for ROI-1 improves with PPM (N = 10) compared to the time-equivalent averaging technique, while the SNR for ROI-2 decreases. This decrease occurs because the signal amplitude in ROI-2 is significantly lower than that of the background noise, and the short code length (N = 10) results in a PA signal with high artifacts, further reducing the SNR. When a denoising autoencoder is applied to the decoded PA signal from PPM (N = 10), it successfully extracts the relatively high-amplitude signal from ROI-1. However, the significantly lower amplitude signal from ROI-2 is lost, as shown in Fig. 15(d). In this figure, the SNR for ROI-1 is 19 dB, while the SNR for ROI-2 drops to –5 dB. Additionally, the presence of strong artifact signals from the short code length of PPM-coded excitation, combined with significant background noise, produces unwanted signals after applying the denoising autoencoder, as illustrated in Fig. 15(d).

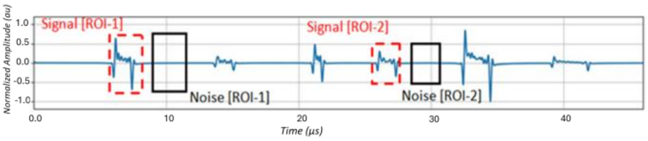

(a) PA signal without noise.

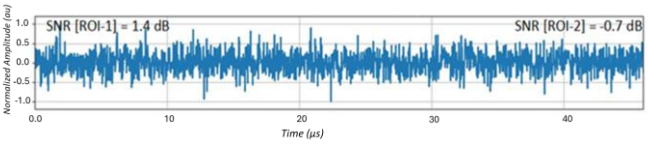

(b) Time-equivalent averaging.

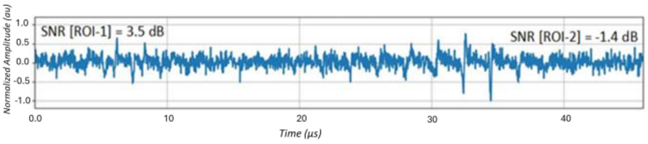

(c) PPM (N=10).

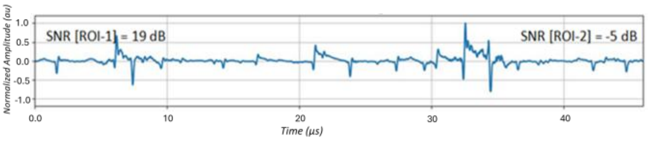

(d) PPM (N=10) and denoising autoencoder.

Fig. 15. (a) Original PA signals; (b) PA signals from time equivalent averaging; (c) PA signals from PPM (N = 10) coded excitation; (d) PA signals from PPM (N = 10) coded excitation with denoising autoencoder.

The performance of the denoising autoencoder on the decoded PA signal from PPM-coded excitation improves as code length increases, as shown in Fig. 16. When the code length is set to 56, the SNR of the decoded PA signal for ROI-1 and ROI-2 icreases by 5.3 dB and 2.6 dB, respectively, compared to the SNR of the PA signal generated by the time-equivalent averaging technique (Fig. 16(b)). The application of the denoising autoencoder further increases the SNR for ROI-1 and ROI-2 by 22.3 dB and 25 dB, respectively, as shown in Fig. 16(d). In addition, the low-amplitude signal in ROI-2 is effectively extracted, and most unwanted signals are removed. However, when comparing the PA signal generated by PPM (N = 56) with the denoising autoencoder (Fig. 16(d)) to the original PA signal (Fig. 16(a)), it is evident that some high-frequency components of the PPM signal are lost. This loss occurs because the denoising autoencoder has difficulty distinguishing these high-frequency parts of the original signal from unwanted signals, such as side lobes and background noise.

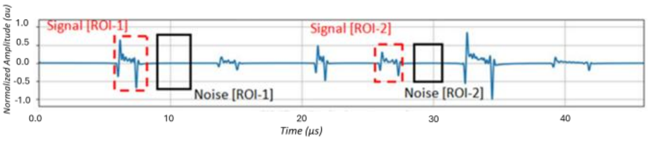

(a) PA signal without noise.

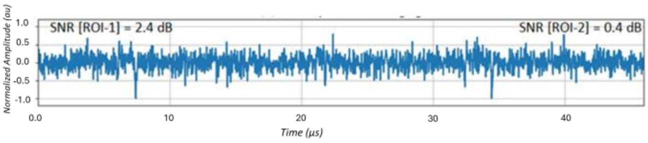

(b) Time-equivalent averaging.

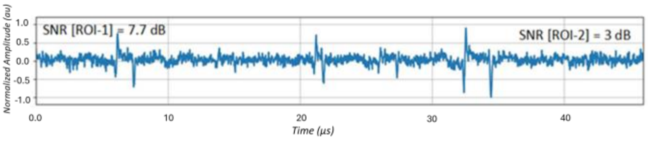

(c) PPM (N=56).

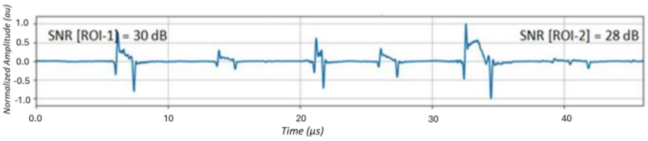

(d) PPM (N=56) and denoising autoencoder.

Fig. 16. (a) Original PA signals; (b) PA signals from time-equivalent averaging; (c) PA signals from PPM (N = 56) coded excitation; (d) PA signals from PPM (N = 56) coded excitation with denoising autoencoder.

4. DISCUSSION

The simulation results show that the denoising autoencoder improves the performance of PPM-coded excitation by reducing background noise and artifact signals (side lobes) in the decoded PA signal. However, when the amplitude of the decoded PA signal is approximately equal to or less than the amplitude of the background noise, the denoising autoencoder has difficulty distinguishing the real PA signal from the noise. This may result in the loss of the real PA signal after applying the denoising autoencoder. To increase the amplitude of the decoded PA signal relative to the background noise, the code length should be increased. This adjustment improves the performance of the denoising autoencoder, as shown in Fig. 17.

When the code length is set to 10, the background noise significantly exceeds the amplitude of the PA signal in the ROI, resulting in the loss of that part of the signal after applying the denoising autoencoder. In contrast, increasing the code length to 40 raises the amplitude of the decoded PA signal above the noise level, enabling successful extraction of the PA signal in the ROI after applying the denoising autoencoder. Using the denoising autoencoder can achieve an SNR greater than that obtained with PPM-coded excitation at the maximum code length for the highest code gain. For example, in the second simulation setup, the mean SNR for the PA signals in ROI-1 and ROI-2 when using PPM with maximum code length was approximately 8 dB and 3 dB, respectively. In comparison, the mean SNR for the PA signals in ROI-1 and ROI-2 when using PPM (N = 40) with the denoising autoencoder was 33 dB and 26 dB, respectively. This demonstrates that using a denoising autoencoder allows PPM-coded excitation to require less acquisition time and data to achieve a specific SNR.

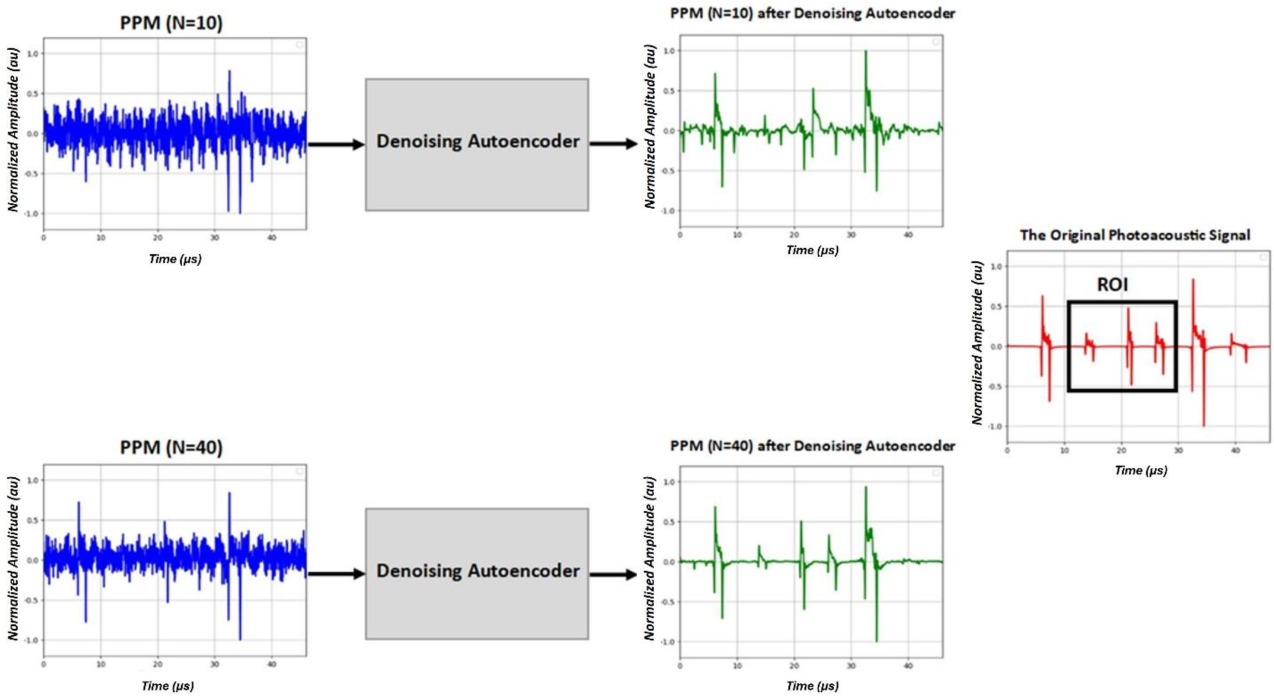

Fig. 17. Effect of code length on the performance of the denoising autoencoder.

5. CONCLUSIONS

In this study, a denoising autoencoder was used to effectively reduce artifacts (side lobes) associated with PPM-coded excitation and to minimize background noise. The denoising autoencoder significantly improves the SNR of PA signals, even with shorter code lengths, resulting in reduced acquisition time and lower memory requirements for RF data collection during decoding. Each PPM code length had a dedicated denoising autoencoder model to address the different shapes of side lobes. The results show that the performance of the denoising autoencoder in attenuating and removing artifacts and background noise improves when the amplitude of the decoded PA signal is greater than that of the background noise. It is important to note that this study was conducted using a simulation setup. Future work will combine the denoising autoencoder and PPM-coded excitation in real experimental settings.

ACKNOWLEDGMENT

The authors would like to thank Ongoing Research Funding Program (ORFFT-2025-111-1), King Saud University, Riyadh, Saudi Arabia for financial support.

REFERENCES

[1] Beard, P. (2011). Biomedical PA imaging. *Interface Focus*, 1 (4), 602-631. https://doi.org/10.1098/rsfs.2011.0028

[2] Wang, L.V., Hu, S. (2012). Photoacoustic tomography: In vivo imaging from organelles to organs. *Science*, 335 (6075), 1458-1462. https://doi.org/10.1126/science.1216210

[3] Xu, M., Wang, L. V. (2006). Photoacoustic imaging in biomedicine. *Review of Scientific Instruments*, 77, 041101. https://doi.org/10.1063/1.2195024

[4] Upputuri, P. K., Pramanik, M. (2016). Recent advances toward preclinical and clinical translation of photoacoustic tomography: A review. *Journal of Biomedical Optics*, 22 (4), 041006. https://doi.org/10.1117/1.JBO.22.4.041006

[5] Wang, T., Nandy, S., Salehi, H. S., Kumavor, P. D., Zhu, Q. (2014). A low-cost photoacoustic microscopy system with a laser diode excitation. *Biomedical Optics Express*, 5 (9), 3053-3058. https://doi.org/10.1364/BOE.5.003053

[6] Upputuri, P. K., Pramanik, M. (2015). Performance characterization of low-cost, high-speed, portable pulsed laser diode photoacoustic tomography (PLD-PAT) system. *Biomedical Optics Express*, 6 (10), 4118-4129. https://doi.org/10.1364/BOE.6.004118

[7] Upputuri, P. K., Pramanik, M. (2015). Pulsed laser diode based optoacoustic imaging of biological tissues. *Biomedical Physics & Engineering Express*, 1, 045010. https://doi.org/10.1088/2057-1976/1/4/045010

[8] Gonzalez, R. C., Woods, R. E. (2019). *Digital Image Processing, Fourth Edition*. Pearson, ISBN 978-9353062989.

[9] Mienkina, M. P., Friedrich, C.-S., Gerhardt, N. C., Wilkening, W. G., Hofmann, M. R., Schmitz, G. (2010). Experimental evaluation of photoacoustic coded excitation using unipolar Golay codes. *IEEE Transactions on Ultrasonics, Ferroelectrics, and Frequency Control*, 57 (7), 1583-1593. https://doi.org/10.1109/TUFFC.2010.1588

[10] Mienkina, M. P., Friedrich, C.-S., Gerhardt, N. C., Beckmann, M. F., Schiffner, M. F., Hofmann, M. R., Schmitz, G. (2010). Multispectral photoacoustic coded excitation imaging using unipolar orthogonal Golay codes. *Optics Express*, 18 (9), 9076-9087. https://doi.org/10.1364/OE.18.009076

[11] Beckmann, M. F., Schmitz, G. (2013). Photoacoustic coded excitation using pulse position modulation. In *2013 IEEE International Ultrasonics Symposium (IUS)*. IEEE, 1853-1856. https://doi.org/10.1109/ULTSYM.2013.0472

[12] Allman, D., Reiter, A., Bell, M. A. L. (2018). Photoacoustic source detection and reflection artifact removal enabled by deep learning. *IEEE Transactions on Medical Imaging*, 37 (6), 1464-1477. https://doi.org/10.1109/TMI.2018.2829662

[13] Lee, S.-E., Park, J., Kim, H.-J., Song, S.-J. (2023). Extraction of flaw signals from the mixed 1-D signals by denoising autoencoder. *Applied Sciences*, 13 (6), 3534. https://doi.org/10.3390/app13063534

[14] Abouzid, H., Chakkor, O., Reyes, O. G., Ventura, S. (2019). Signal speech reconstruction and noise removal using convolutional denoising audioencoders with neural deep learning. *Analog Integrated Circuits and Signal Processing*, 100, 501-512. https://doi.org/10.1007/s10470-019-01446-6

[15] Fusco, A., Krueger, M., Servadei, L., Wille, R. (2023). A deep learning approach for artifact suppression in MEMS-based airborne ultrasonic transceivers. In *2023 IEEE International Ultrasonics Symposium (IUS)*. IEEE. https://doi.org/10.1109/IUS51837.2023.10308240

[16] Treeby, B. E., Jaros, J., Cox, B. T. (2016). Advanced photoacoustic image reconstruction using the k-Wave toolbox. In *Photons Plus Ultrasound: Imaging and Sensing 2016*. SPIE, 9708, 517-530. https://doi.org/10.1117/12.2209254

[17] Treeby, B. E., Zhang, E. Z., Cox, B. T. (2010). Photoacoustic tomography in absorbing acoustic media using time reversal. *Inverse Problems*, 26 (11), 115003. https://doi.org/10.1088/0266-5611/26/11/115003

[18] Glorot, X., Bordes, A., Bengio, Y. (2011). Deep sparse rectifier neural networks. In *Proceedings of the Fourteenth International Conference on Artificial Intelligence and Statistics*. JMLR, 15, 315-323.

[19] Srivastava, N., Hinton, G., Krizhevsky, A., Sutskever, I., Salakhutdinov, R. (2014). Dropout: A simple way to prevent neural networks from overfitting. *Journal of Machine Learning Research*, 15 (56), 1929-1958.

[20] Heinz, C., Reiner, M., Belka, C., Walter, F., Söhn, M. (2015). Technical evaluation of different respiratory monitoring systems used for 4D CT acquisition under free breathing. *Journal of Applied Clinical Medical Physics*, 16 (2), 334-349. https://doi.org/10.1120/jacmp.v16i2.4917

Received March 7, 2025
Accepted October 20, 2025